Supporting information

Structural and electronic engineering of biomass-derived carbon nanosheets for electrochemical oxygen reduction

Kristina Maliutina[a,b], Changjie He[a], Jiajia Huang[a], Jianglong Yu[c], Fengjiao Li[a], Chuanxin He[a],

Liangdong Fan[a,d]**

[a]College of Chemistry and Environmental Engineering, Shenzhen University, Shenzhen 518060,

Guangdong, China

[b]College of Physics and Optoelectronic Engineering, Key Lab of Optoelectronic Devices and

Systems of Ministry of Education/Guangdong Province, Shenzhen University, Shenzhen 518060,

Guangdong, China.

[c]Department of Chemical Engineering, University of Newcastle, Callaghan, NSW 2308,

Australia

[d]Shenzhen Key Laboratory of New Lithium-ion Batteries and Mesoporous Materials, Shenzhen

University, Shenzhen 518060, Guangdong, China.

Number of figures: 13

Number of tables: 4

*Corresponding author: fanld@szu.edu.cn (Fan L.D.)

Biomass drying, crushing, sieving

Alkaline Treatment with 5%NaOH

Acid Hydrolysis with 1% H₂SO₄ at 70°C
Washing pH=7 with 5%NaOH

Filtration/Centrifugation
Freeze-drying: -80°C and -20°C for 48 h

Trithiocyanuric acid doping
Microwave pyrolysis
Biochar collection

Raw PP

Cell-PP

Cell-PP-NS-700
- **Pyrrolic-N**
- **Pyridinic-N**
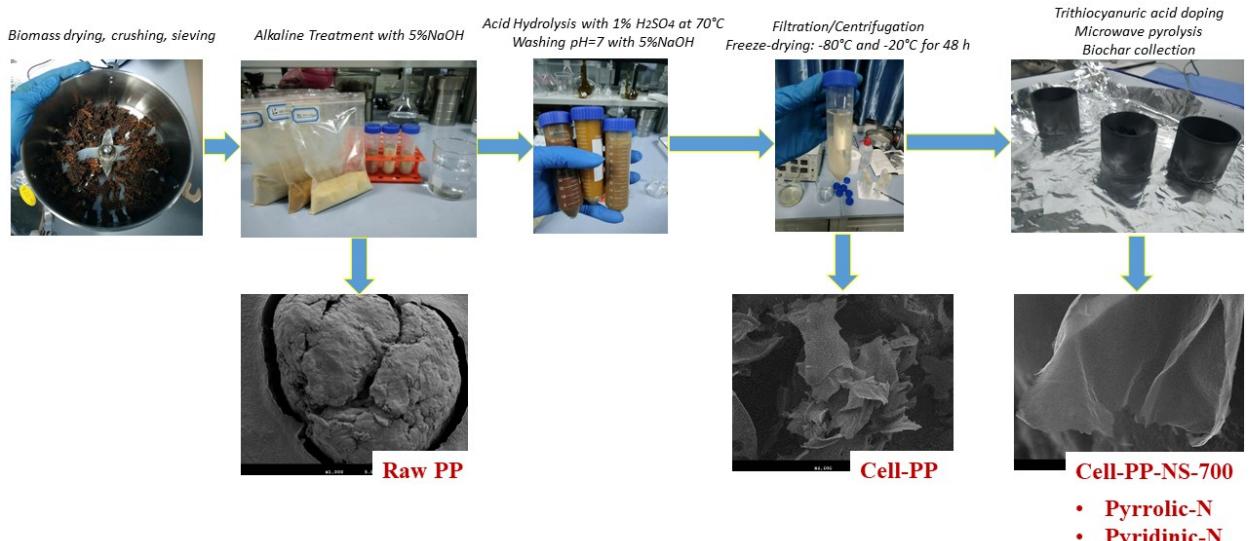
Fig. S1. Detailed diagram of the pretreatment process for the production of the cell-PP-NS-700 biochar precursor.
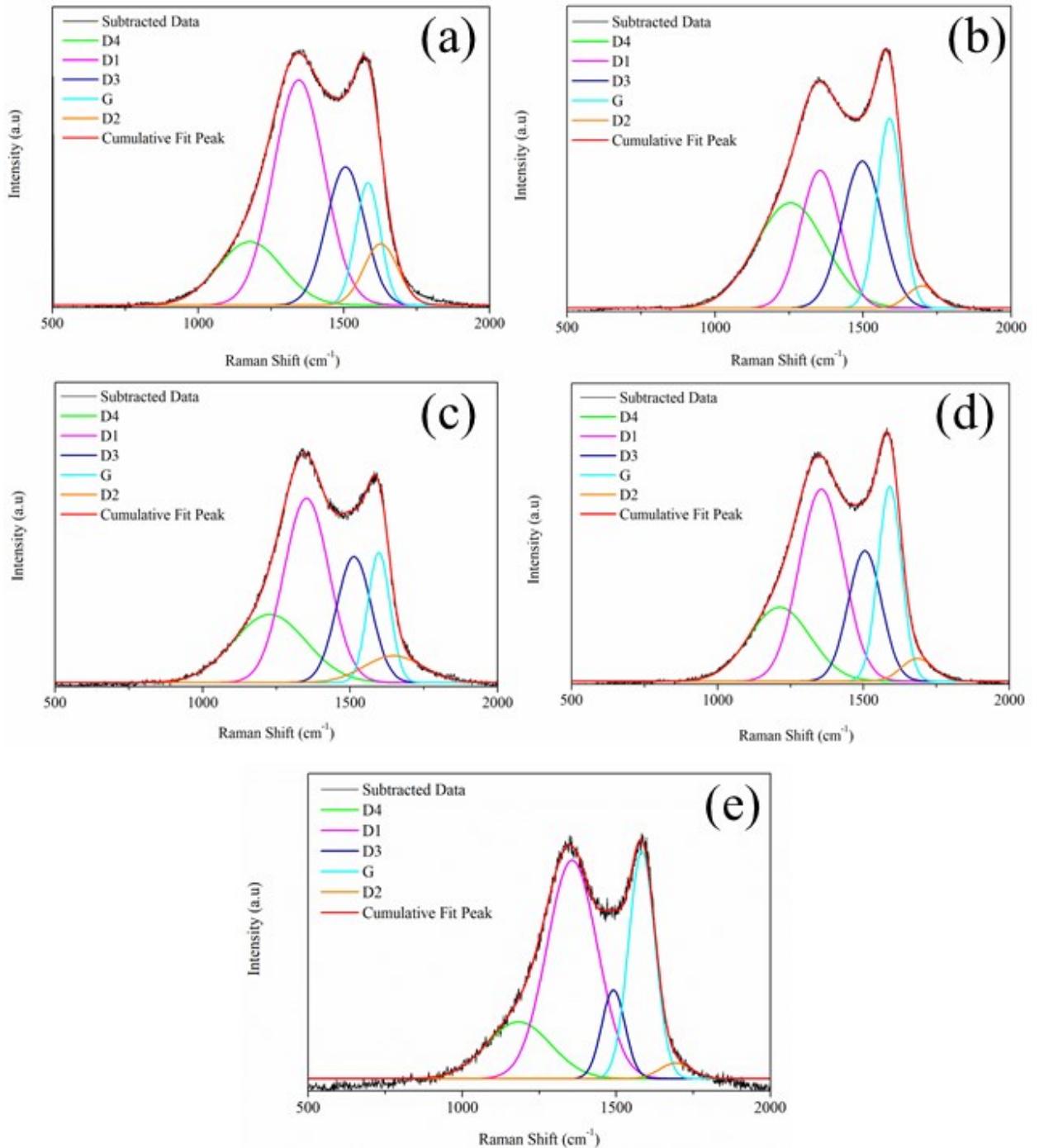
Fig. S2. Curve-fitted Raman spectra, corresponding to (a) Raw PP, (b) cell-PP, (c) cell-PP-NS-700, (d) cell-PP-NS-700-Ta and (e) cell-PP-NS-700-Ta-900 samples.
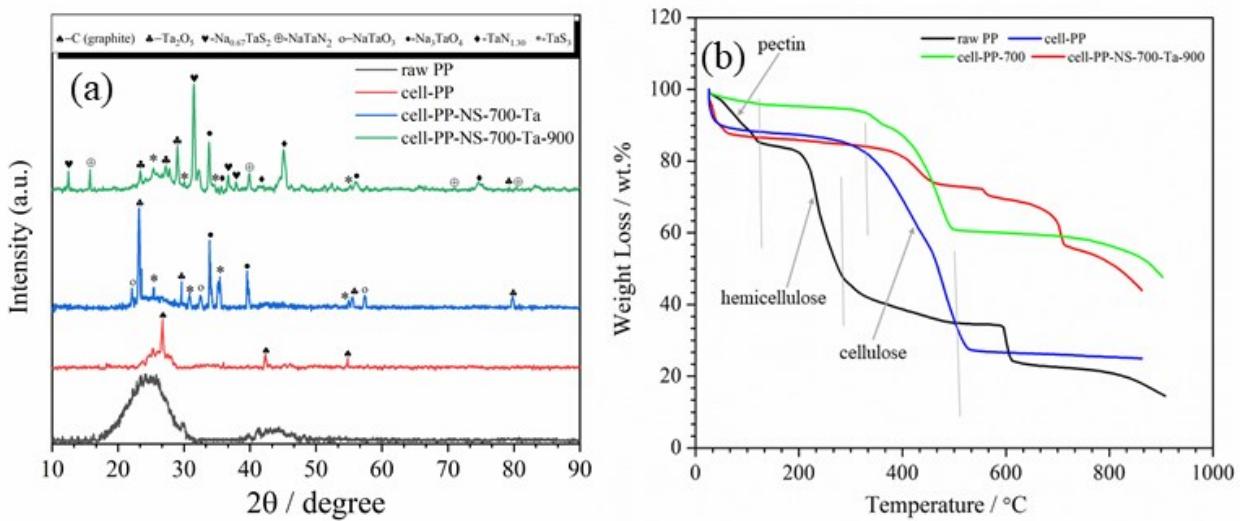
Fig. S3. The normalized spectrum of (a) XRD patterns and (b) TG decomposition curves in air atmosphere of the catalyst precursor and as-prepared catalysts.
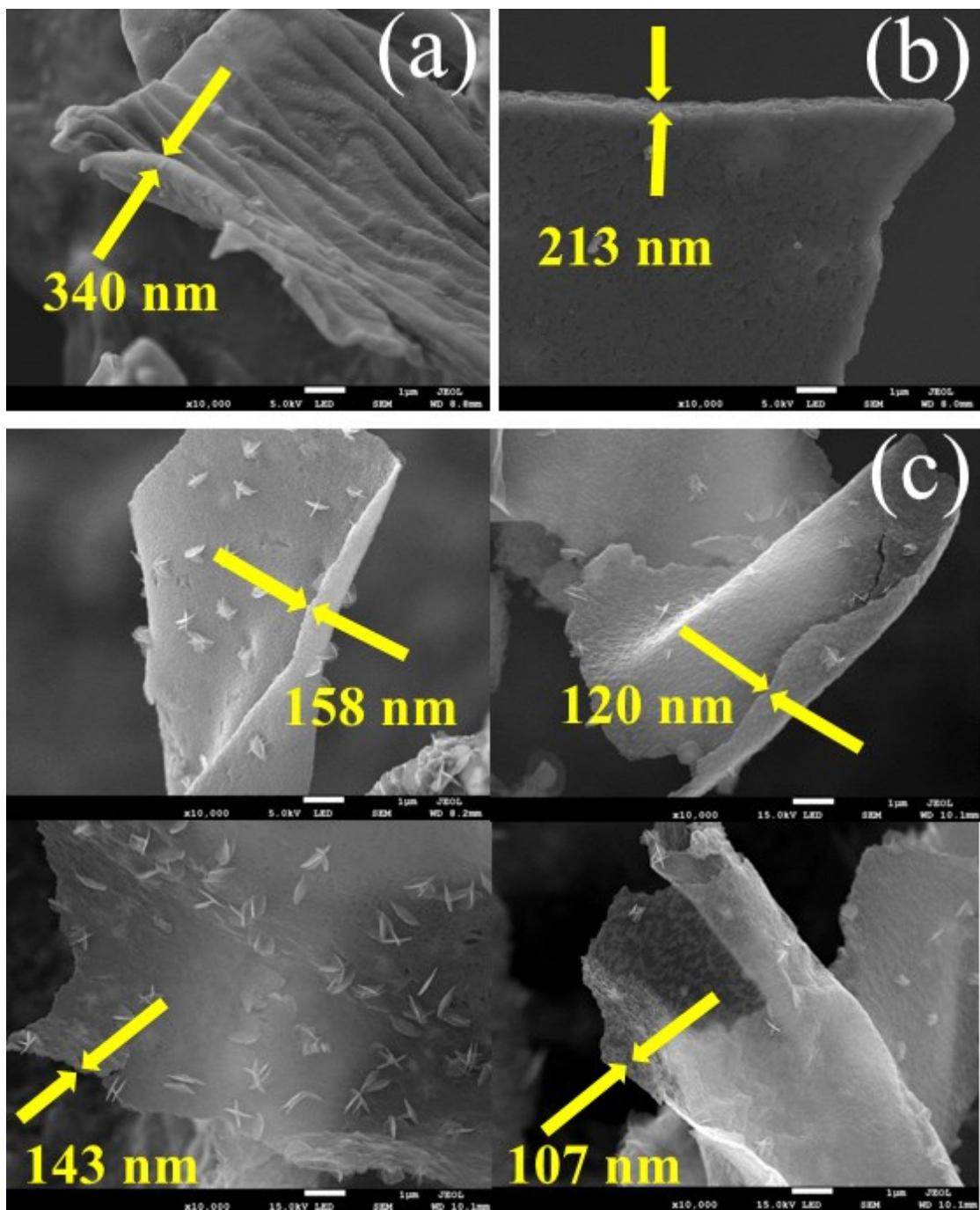
Fig. S4. Variety of FE-SEM images for representative nanosheet-like samples of (a) cell-PP; (b) cell-PP-NS-700; (c) cell-PP-NS-700-Ta-900.
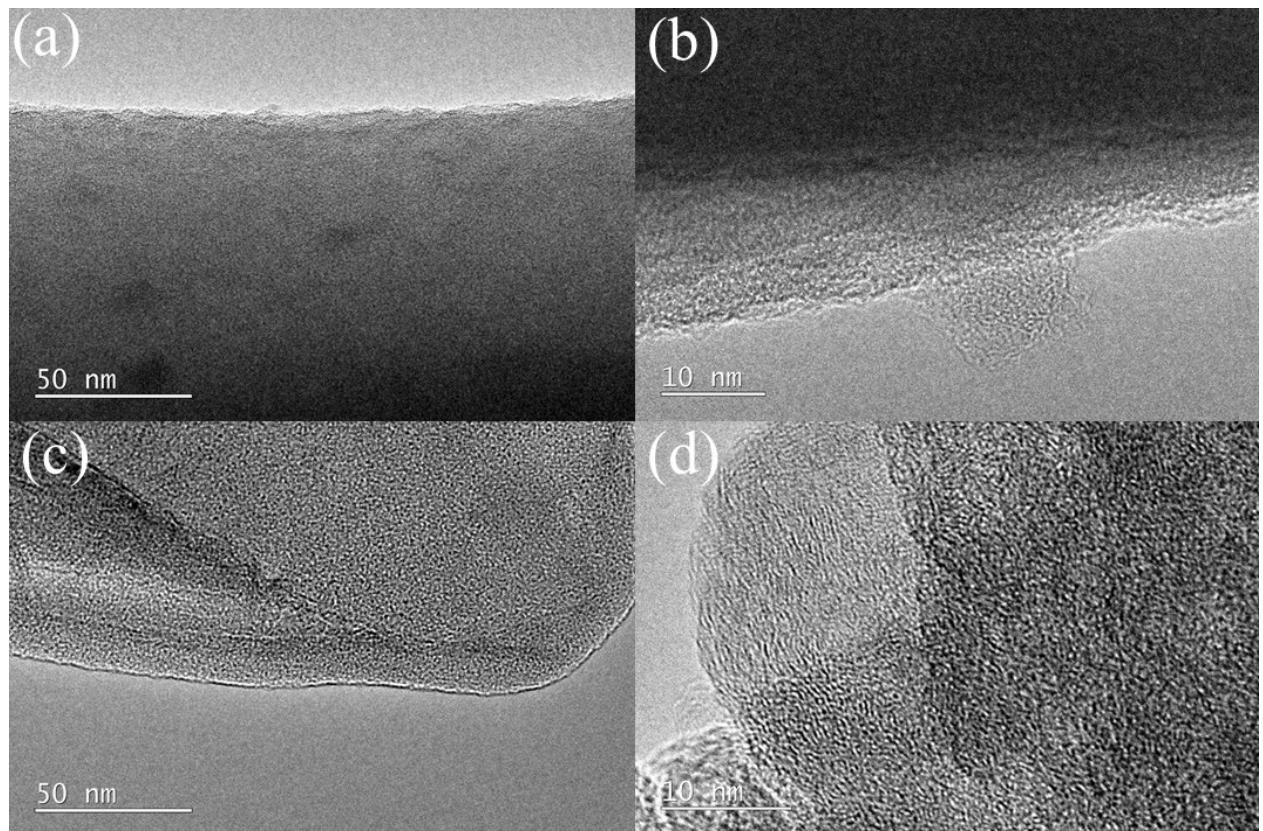
Fig. S5. TEM images of (a,b) cell-PP-700 and (c,d) cell-PP-NS-700 samples corresponding for porosity at different magnifications.
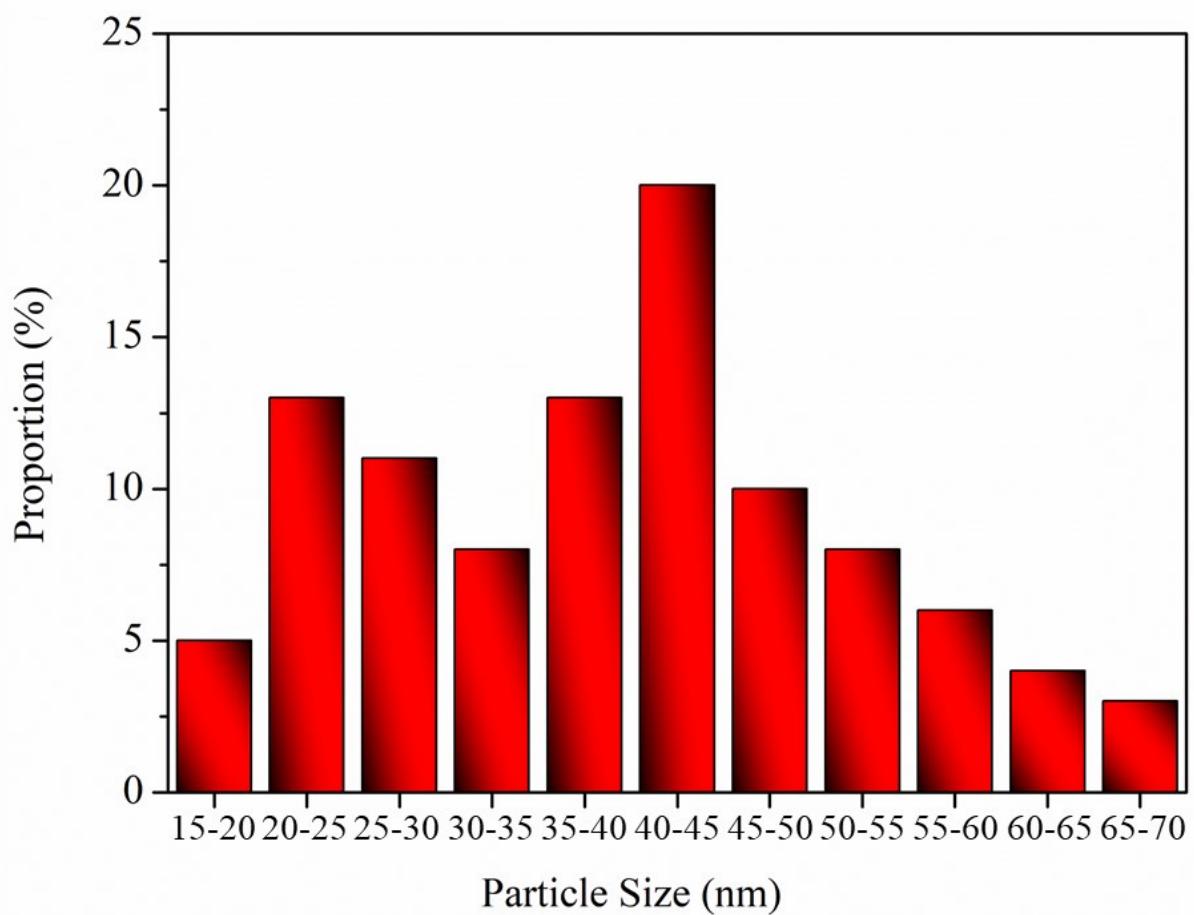
Fig. S6. The particle size distribution of the Ta-based nanoparticles on the cell-PP-NS-700-Ta-900 nanosheet electrocatalyst
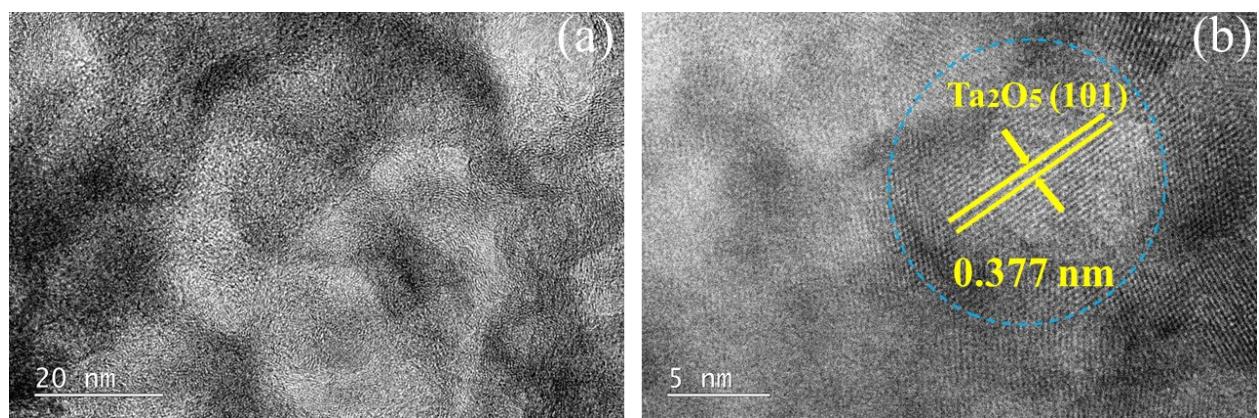
Fig. S7. TEM image (a) and magnified HR-TEM images (b) of the cell-PP-700-Ta-900 catalyst.
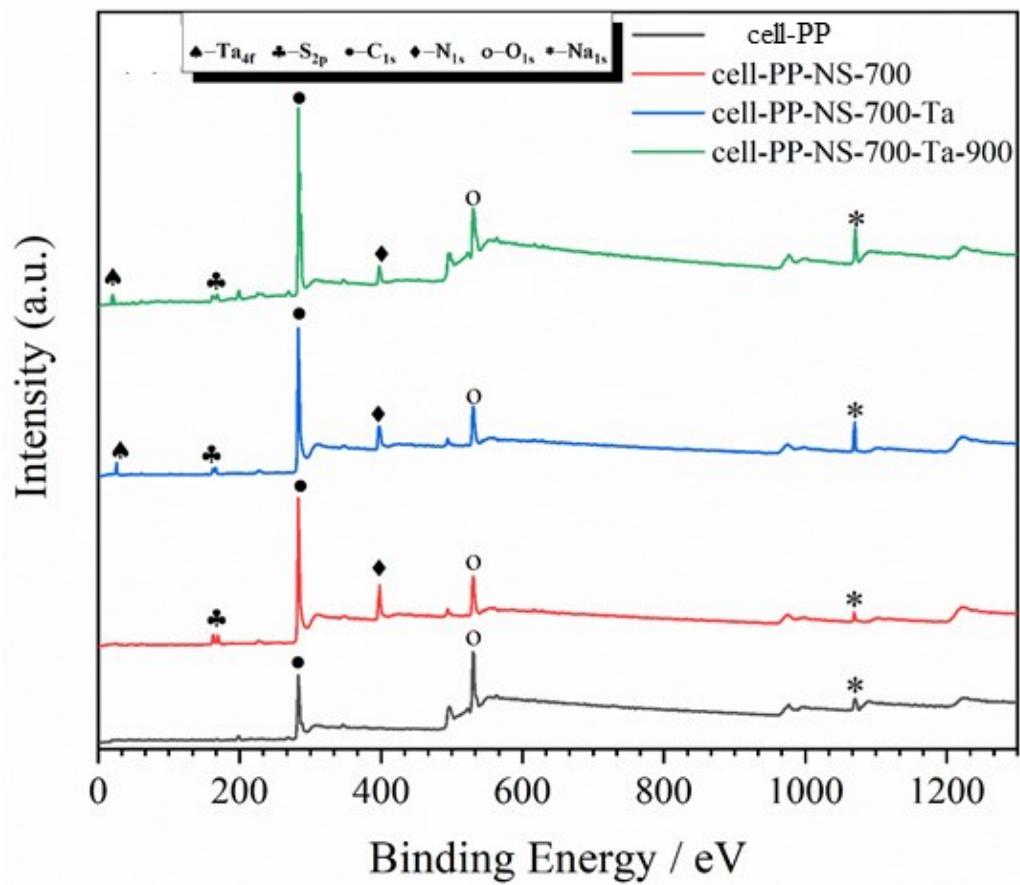
**Fig. S8.** The normalized spectrum of XPS survey for cell-PP precursor and as-prepared catalysts.
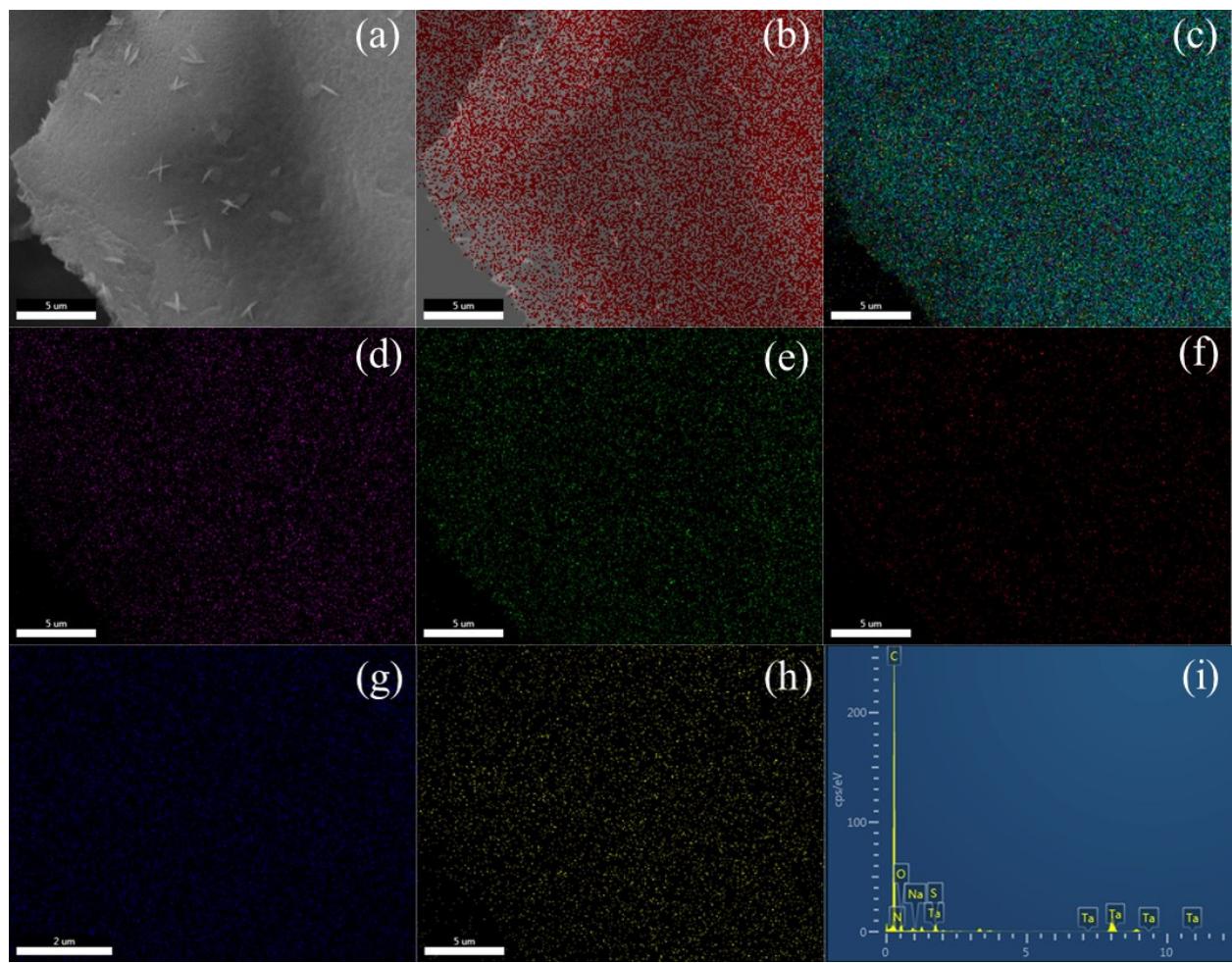
Fig. S9. SEM-EDAX analysis for cell-PP-NS-700-Ta-900 catalyst with corresponding images of (a) SEM micrograph of the scanned area; (b) the survey spectra of the EDAX-mapping for all the elements, (c) C, (d) N, (e) O, (f) Na, (g) Ta, (h) S and (i) the EDAX spectra for the cell-PP-NS-700-Ta-900 catalyst.
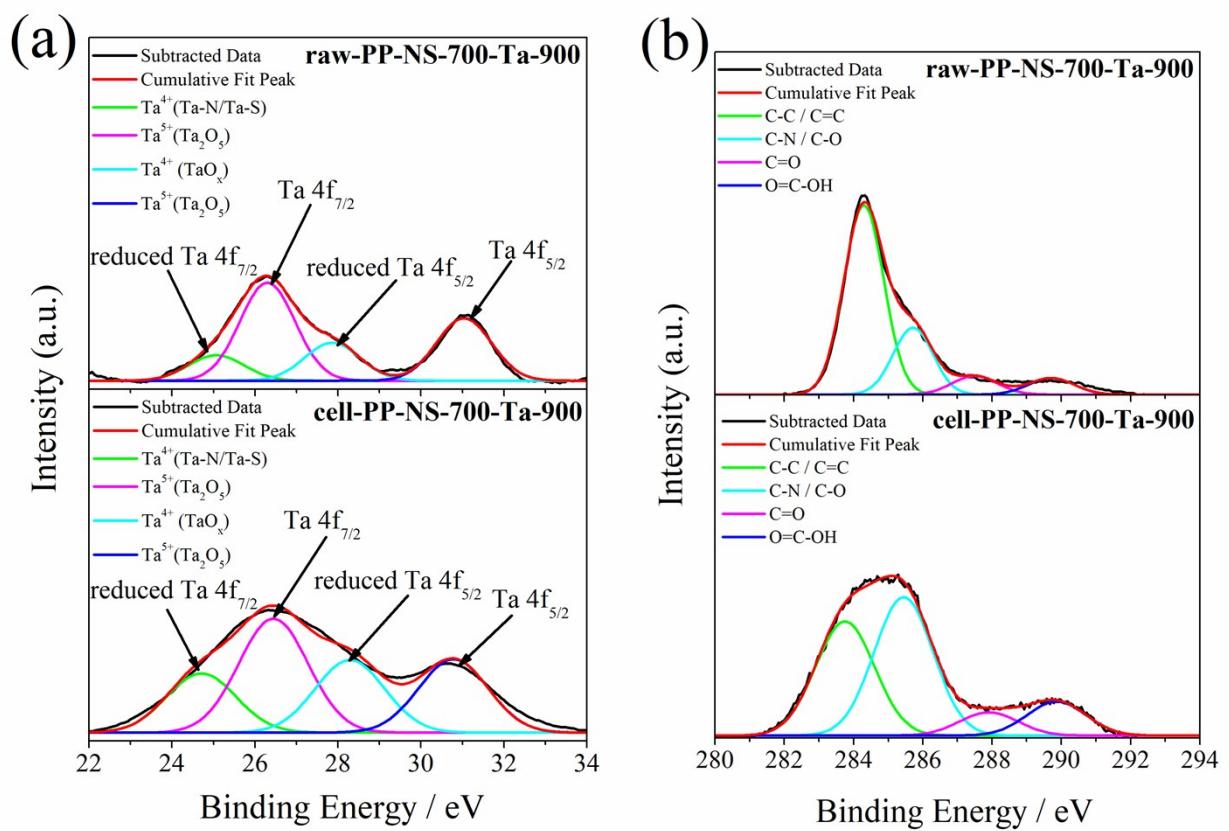
Fig. S10. XPS high-resolution curve-fitting spectra for the raw-PP-NS-700-Ta-900 and cell-PP-NS-700-Ta-900 samples attributed to (a) Ta 4f and (b) C 1s patterns.
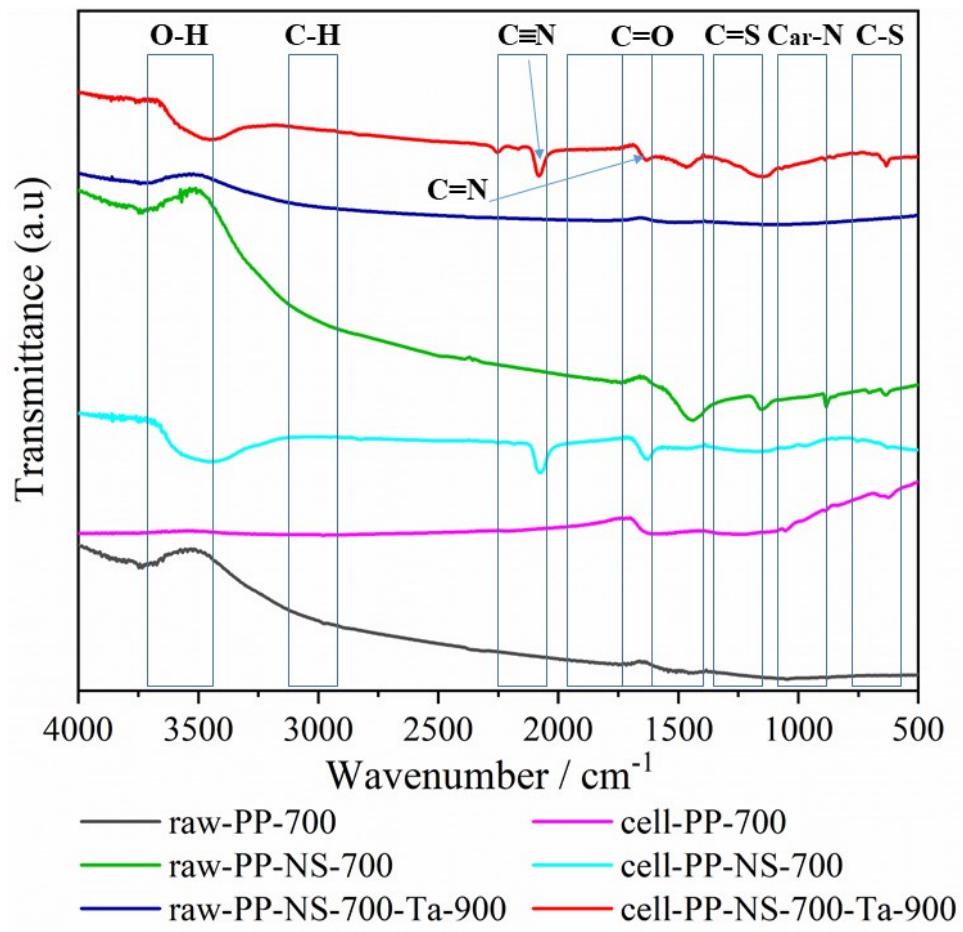
Fig. S11. Normalized FT-IR spectra of the raw PP bio-char, pretreated cell-PP bio-char and as-

prepared catalysts.
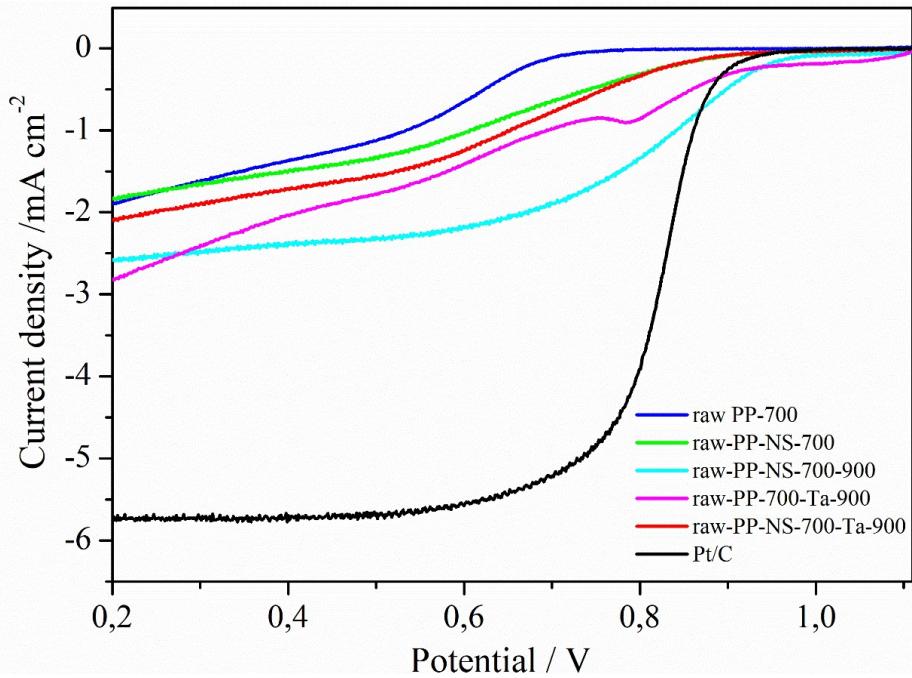
Fig. S12. RDE polarization curves for the serious of raw-PP biomass-derived catalysts performed in O_2 saturated 0.1 M KOH with a scanning rate of 5 mV s^{-1}.
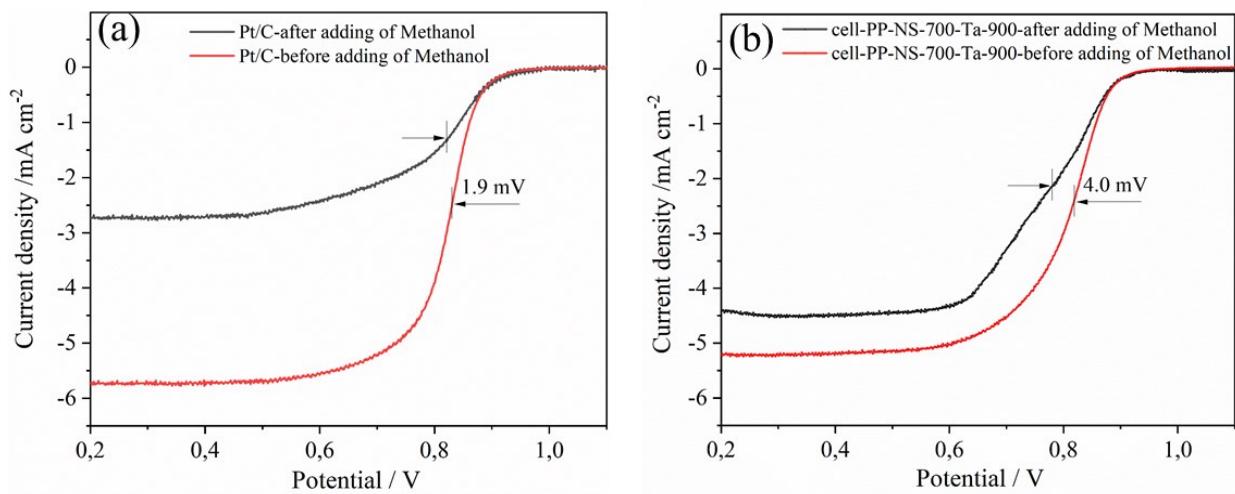
Fig. S13. LSV curves in O_2 saturated 0.1 M KOH at 5 mV s^{-1} and 1600 rpm before and after methanol poisoning for Pt/C (a) and cell-PP-NS-700-Ta-900 (b).

Table S1. The main functional bands determined by the Raman spectroscopy

Band	Raman shift (cm^{-1})	Vibration mode
D4	~1150-1180	C–C and C=C stretching vibrations of the disordered graphitic frame (polyene-like structures, and/or ionic contaminants)
D1	~1340-1350	In-plane imperfections in such as defects in the graphitic lattice or graphene layers and heteroatoms
D3	~1500-1530	Organic molecules, fragments or functional groups in poorly organized materials (amorphous carbon) responsible for active sites
G	~1580	Graphitic structures (E_{2g} symmetry)
D2	~1600-1620	Lattice vibration of disordered graphitic lattice involving graphene layers

Table S2. The atomic percentage (%) results for the raw PP biomass and its derivatives performed by XPS analysis

Sample	Carbon content (at.%)	Nitrogen content (at.%)	Sulphur content (at.%)	Sodium content (at.%)	Tantalum content (at.%)	Oxygen content (at.%)
raw PP	55.80	0.55	0.31	3.90	-	39.44
cell-PP	66.61	0.11	0.88	5.90	-	26.50
cell-PP-700	71.75	0.21	0.46	4.32	-	23.26
cell-PP-700-Ta	72.06	0.65	0.24	7.98	6.11	12.96
cell-PP-700-Ta-900	71.99	0.33	0.11	7.54	6.48	13.55
cell-PP-NS-700	67.13	8.28	4.55	3.19	-	16.85
cell-PP-NS-700-900	77.96	1.14	1.88	3.99	-	15.03
cell-PP-NS-700-Ta	66.36	7.71	4.70	7.76	4.89	8.58
cell-PP-NS-700-Ta-900	69.11	4.88	3.04	6.08	6.17	10.72

Table S3. Ultimate analysis (wt%, daf) of raw PP biomass, cell-PP precursor and its derivatives

Sample	C	N	H	S	O*
raw PP	36.16+0.81	2.11±0.22	9.55±0.90	0.44±0.13	51.74±0.77
cell-PP	47.06±0.55	1.11±0.13	6.89±0.77	1.18±0.11	43.76±1.13
cell-PP-700	59.92±1.03	1.08±0.15	2.44±0.50	0.55±0.19	36.01±0.55
cell-PP-NS-700	57.77±0.88	11.66±0.18	2.41±0.76	6.31±0.66	21.85±0.96
cell-PP-NS-700-Ta	58.84±0.97	10.23±1.12	2.66±0.48	5.89±0.71	22.38±1.17
cell-PP-700-Ta-900	72.05±0.77	0.88±0.25	3.71±0.11	0.50±0.11	22.86±0.44
cell-PP-NS-700-Ta-900	71.18±0.49	4.16±0.80	2.08±0.63	2.53±0.32	20.05±0.81

* by difference; daf: dry ash free

Table S4. Comparison of ORR catalytic properties of the cell-PP-NS-799-Ta-900 catalyst, Pt/C benchmark catalyst and other tantalum-contained electrocatalysts. Rotating disk electrode (RDE) results in terms of onset potential (E_{onset}), half-wave potential ($E_{1/2}$), and the limited current density (J_L) in O_2 saturated environments and 1600 rpm

Catalyst	Test conditions	E_{onset} (V vs. RHE)	$E_{1/2}$ (V vs. RHE)	J_L (mA cm^{-2})	Ref.
Pt/C	0.1 M KOH, 5 mV s^{-1}	0.9420	0.83	-5.73	Current
Cell-PP-NS-700-Ta-900	0.1 M KOH, 5 mV s^{-1}	0.931	0.82	-5.24	work
TaC$_x$N$_y$O$_z$/MWCNT	0.1 M H$_2$SO$_4$, 5 mV s^{-1}	0.900	0.76	-3.12	[1]
Core-shell TaON@CN-1000	0.1 M KOH, 10 mV s^{-1}	0.800	0.70	-4.30	[2]
	0.5 M H$_2$SO$_4$, 10 mV s^{-1}	0.700	0.48	-2.50	
Ta–CNO	0.1 M H$_2$SO$_4$, 5 mV s^{-1}	0.800	0.72	-3.10	[3]
TaOx/C900	0.5 M H$_2$SO$_4$, 5 mV s^{-1a}	0.460	0.32	-2.70	[4]
TaOx/CB-873K, 2h	0.1 M KOH, 5mV s^{-1}	0.950	0.73	-	[5]
Pt/TaO$_x$/GC	0.1 M HClO$_4$, 5 mV s^{-1}	0.950	0.80	-6.0	[6]
Partially oxidized Ta–CN powders	0.1 M H$_2$SO$_4$, 5 mV s^{-1}	0.940	0.60	-0.7	[7]
TaOxNy-800	0.1 M H$_2$SO$_4$, 5 mV s^{-1}	0.750	0.40	-	[8]
Reduced Ta$_2$O$_5$	0.1 M H$_2$SO$_4$, 5 mV s^{-1}	0.800	0.68	-	[9]
TaO$_x$ in form of Na$_2$Ta$_8$O$_{21-x}$ /G900	0.5 M H$_2$SO$_4$, 5 mV s^{-1}	0.800	0.45	-1.0	[10]
Ta-CNO-1000C	0.1 M H$_2$SO$_4$, 5 mV s^{-1}	0.800	0.60	-	[11]
N-doped TaO$_x$/RGO-775	0.1 M KOH, 5mV s^{-1}	0.880	0.80	-4.4	[12]
TaO$_x$ in form of Na$_2$Ta$_8$O$_{21-x}$ /C-3%-1000	0.1 M KOH, 5mV s^{-1}	0.800	0.65	-2.0	[13]

[a]A saturated calomel electrode (Hg|Hg$_2$Cl$_2$, sat. KCl) was used as the reference electrode

References

1   N. Uehara, A. Ishihara, T. Nagai, M. Matsumoto, H. Imai, Y. Kohno, K. Matsuzawa, S. Mitsushima and K. Ota, Kinetic study of oxygen reduction reaction on tantalum oxide-based electrocatalysts produced from oxy-tantalum phthalocyanines in acidic media, *Electrochim. Acta* 2015, **182**, 789-794.

2   M. Wassner, M. Eckardt, C. Gebauer, G. R. Bourret, N. Hüsing and R. J. Behm, Synthesis and electrocatalytic performance of spherical core-shell tantalum (oxy)nitride@nitrided carbon composites in the oxygen reduction reaction, *Electrochim. Acta* 2017, **227**, 367-381.

3   K. Matsuzawa, K. Nozawa, K. Yamauchi, A. Ishihara, S. Mitsushima and K.-i. Ota, Immersed effects of Ta and Zr compounds on activity of oxygen reduction reaction in sulfuric acid, *J. Power Sources* 2013, **226**, 16-19.

4   D. Sebastián, V. Baglio, S. Sun, A. C. Tavares and A. S. Aricò, Facile synthesis of Zr- and Ta-based catalysts for the oxygen reduction reaction, *Chin. J. Catal.* , 2015, **36**, 484-489.

5   J. Seo, D. H. Anjum, K. Takanabe, J. Kubota and K. Domen, Electrodeposited Ultrafine TaOx/CB Catalysts for PEFC Cathode Application: Their Oxygen Reduction Reaction Kinetics, *Electrochim. Acta* 2014, **149**, 76-85.

6   Z. Awaludin, M. Suzuki, J. Masud, T. Okajima and T. Ohsaka, Enhanced Electrocatalysis of Oxygen Reduction on Pt/TaOx/GC, *J. Phys. Chem. C*, 2011, **115**, 25557-25567.

7   A. Ishihara, M. Tamura, K. Matsuzawa, S. Mitsushima and K.-i. Ota, Tantalum oxide-based compounds as new non-noble cathodes for polymer electrolyte fuel cell, *Electrochim. Acta* 2010, **55**, 7581-7589.

8   A. Ishihara, S. Doi, S. Mitsushima and K.-i. Ota, Tantalum (oxy)nitrides prepared using reactive sputtering for new nonplatinum cathodes of polymer electrolyte fuel cell, *Electrochim. Acta* 2008, **53**, 5442-5450.

9   Z. Awaludin, T. Okajima and T. Ohsaka, Preparation of reduced tantalum pentoxide by electrochemical technique for oxygen reduction reaction, *J. Power Sources* 2014, **268**, 728-732.

10   D. Sebastián, V. Baglio, S. Sun, A. C. Tavares and A. S. Aricò, Graphene-Supported Substoichiometric Sodium Tantalate as a Methanol-Tolerant, Non-Noble-Metal Catalyst for the Electroreduction of Oxygen, *ChemCatChem* 2015, **7**, 911-915.

11   A. Ishihara, M. Tamura, Y. Ohgi, M. Matsumoto, K. Matsuzawa, S. Mitsushima, H. Imai and K.-i. Ota, Emergence of Oxygen Reduction Activity in Partially Oxidized Tantalum Carbonitrides: Roles of Deposited Carbon for Oxygen-Reduction-Reaction-Site Creation and Surface Electron Conduction, *J. Phys. Chem. C*, 2013, **117**, 18837-18844.

12   X. Yang, Q. Mo, Y. Guo, N. Chen and Q. Gao, Reduced-graphene-oxide supported tantalum-based electrocatalysts: Controlled nitrogen doping and oxygen reduction reaction, *Appl. Surf. Sci.* , 2018, **434**, 243-250.

13   J. C. Ruiz-Cornejo, D. Sebastián, M. V. Martínez-Huerta and M. J. Lázaro, Tantalum-based electrocatalysts prepared by a microemulsion method for the oxygen reduction and evolution reactions, *Electrochim. Acta* 2019, **317**, 261-271.